The Arctic Ozone Hole in March 2020 and Its Seasonal Prediction in CFSv2: A Comparative Study with the 1997 and 2011 Arctic Ozone Holes

Jian Rao[1,2] and Chaim I. Garfinkel[1]

[1]Fredy and Nadine Herrmann Institute of Earth Sciences, The Hebrew University of Jerusalem, Edmond J. Safra Campus, Givat Ram Jerusalem 91904, Israel

[2]Key Laboratory of Meteorological Disaster, Ministry of Education (KLME) / Joint International Research Laboratory of Climate and Environment Change (ILCEC) / Collaborative Innovation Center on Forecast and Evaluation of Meteorological Disasters (CIC-FEMD), Nanjing University of Information Science and Technology, Nanjing 210044, China

Submitted to *Geophysical Research Letters*

(May 2020)

Corresponding author: Dr. Jian Rao, jian.rao@mail.huji.ac.il

Key Points:

- The 1997, 2011 and 2020 March ozone holes were accompanied by an extremely strong and cold polar vortex.
- The shape and centroid of the Arctic total ozone holes were controlled by the stratospheric polar vortex.
- The 2011 March ozone hole is more predictable than the 1997 and 2020 March ozone hole events, possibly due to favorable ENSO and QBO conditions.

Abstract

Using reanalysis data, observations, and seasonal forecasts, the March Arctic ozone hole events in 1997, 2011, and 2020 and their predictability are compared. All of the three ozone hole events were accompanied by an extremely strong and cold polar vortex. The shape and centroid of the ozone holes are mainly controlled by the simultaneous polar vortex. The March 2020 ozone hole was displaced towards Canada and Greenland, the March 2011 ozone low was evenly distributed over the North Pole, while the 1997 ozone hole was displaced toward Arctic Russia. The predictability of the 2011 ozone hole event is longer (1–2 months) than the other two (~1 month) possibly due to a moderate La Niña and Quasi-Biennial westerly winds, favorable for the formation of a strong polar vortex. Surprisingly, an empirical model using a substitute index to forecast the Arctic ozone might be as skillful as the general circulation model with a chemistry module.

Key words: Arctic ozone hole; stratospheric polar vortex; predictability

Plain language

Low total column ozone was observed this past March over the Artic (a so-called “ozone hole”), and its meteorological conditions are compared with the other two similar Arctic low-ozone events in 1997 and 2011. All of the three historical ozone hole events occurred within an unusually strong and cold stratospheric polar vortex, and the shape and centroid of the ozone holes were also consistent with the polar vortex. The ozone hole in March 2020 was displaced towards the North American sector, the March 2011 ozone hole was centered over the North Pole, while the 1997 ozone hole displaced toward the Eurasian sector. We also find that the predictability of the 2011 ozone hole event is longer (1–2 months) than the 1997 and 2020 March event (~1 month), perhaps due to favorable tropical forcings (e.g., La Niña and westerly QBO). The general circulation model with a chemical module shows a comparable predictive skill for the ozone holes to an empirical model using a substitute index to forecast the Arctic ozone.

1. Introduction

During the austral spring, a nearly complete depletion of lower-stratospheric ozone results in an ozone hole over the Antarctic nearly every year (Solomon, 1999; Manney et al., 2011; Rieder et al., 2014). In the Northern Hemisphere, on the other hand, chlorine activation and subsequent Arctic ozone depletion only occur when the stratospheric polar vortex persists into spring and lower stratospheric temperatures are unusually cold (Arnone et al., 2012). Arctic ozone loss therefore has large interannual variability due to large planetary wave disturbances and even sudden warmings which ordinarily prevent long-lived cold temperature in the Northern Hemisphere (Manney et al., 2011). Hitherto, only three Northern Hemisphere "ozone hole" events have been observed since 1979 (i.e., March in 1997, 2011, and 2020 in Fig. 1).

The March 1997 ozone hole (Newman et al., 1997; Zhang et al., 2013) and especially the March 2011 ozone hole (Hurwitz et al., 2011; Liu et al., 2011; Sinnhuber et al., 2011; Varotsos et al., 2012; Arnone et al., 2012; Solomon et al., 2014; Chipperfield et al., 2015) have attracted wide attention. For example, Arnone et al. (2012) analyzed the Arctic dynamics, chemistry, and polar stratospheric clouds during the 2010/11 ozone hole using the limb sounding infrared measurements. Two major processes are responsible for the low ozone in early spring over the Arctic: heterogeneous chemical loss (Solomon, 1999; Hommel et al., 2014; Shaw & Perlwitz, 2014) and a quiescent stratosphere in winter (Olascoaga et al., 2012; Strahan et al., 2013). When the stratosphere is quiescent and the stratospheric westerly jet is strong, the poleward mass transport from the ozone-rich tropics to the ozone-poor polar regions is blocked with the anomalously strong jet serving as a barrier for the ozone transport (Strahan et al., 2013). On the other hand, ozone depletion in the Arctic winter is also dependent on the volume of the polar stratosphere below the temperature threshold for polar stratospheric cloud formation (Rex et al., 2006; Harris et al., 2010; Garfinkel et al., 2015). The Arctic stratospheric temperatures in the 2010/11 winter were one of the coldest (Manney et al., 2011; Sinnhuber et al., 2011). The ozone loss over the Arctic in the 2011 spring was quantitatively comparable to that in the Antarctic ozone hole (e.g., Sinnhuber et al., 2011; Varotsos et al., 2012).

Springs with low Arctic (Antarctic) ozone concentration in March (October) are associated with a strong and cold stratospheric polar vortex, which corresponds to the positive polarity of NAM/NAO (SAM) in early boreal (austral) spring (Thompson & Solomon, 2002; Previdi & Polvani, 2014; Solomon et al., 2014). Both modelling and observational evidence show that the extreme low Arctic stratospheric ozone anomalies in spring are usually accompanied with a poleward shift of the tropospheric westerly jet in the North Atlantic sector and a positive NAO-like circulation pattern (Calvo et al., 2015; Ivy et al., 2017), though the surface impacts may be associated more with the strong vortex that allowed for the low ozone in the first place (Harari et al., 2019). In addition, an ozone hole allows for ultraviolet radiation to reach the surface, which endangers the lives of plants, animals, and humans inhabiting the Arctic. Considering the possible impact of the ozone loss on the near-surface weather and ecosystem (Waugh et al., 2009; Neely et al., 2014), a timely

prediction of ozone hole events can be used to warn society.

This paper focuses on the general meteorological conditions for the three historical "ozone hole" events in the Northern Hemisphere, although the ozone holes over the Arctic are not as deep as in the Antarctic. Seasonal predictions of the three ozone hole events are compared using operational model output by an operational forecast system. We will show that the predictability of the ozone hole is largely dependent on the representation of the polar vortex in the forecast system for the three Arctic cases.

The organization of the paper is as follows. Following the introduction, section 2 describes the data, model forecasts, and methods. The background circulation conditions for the three Arctic ozone hole events are shown in section 3. The predictions of the Arctic ozone holes using the empirical method and the forecast model are compared in section 4. Finally, conclusions are presented in section 5.

2. CFSv2 seasonal forecasts, data, and methods

2.1 NCEP Climate Forecast System version 2 (CFSv2) and its seasonal predictions

As a successor to NCEP CFSv1, the NCEP CFSv2 began to operate on 30 March 2011 (Saha et al., 2014). The CFSv2 forecast model is a fully coupled model system with an atmospheric spectral model interacting with ocean, land, and sea ice. The forecast system runs at a T126 (~100 km) horizontal resolution for the atmosphere. This model uses a signal-pressure hybrid vertical coordinate with 64 levels. This model was also used to create the NCEP Climate Forecast System Reanalysis (CFSR). The seasonal reforecasts before 2011 by CFSv2 were performed every five days. The reforecasts initialized on the specific days have four members using the initial conditions at 0000, 0600, 1200, and 1800 UTC. The real-time seasonal forecasts were initialized four times (0000, 0600, 1200, and 1800 UTC) per day. The seasonal forecast/reforecast products produced 9-month integrations (https://www.ncdc.noaa.gov/data-access/model-data/model-datasets/climate-forecast-system-version2-cfsv2). CFSv2 is also one of models participating in the subseasonal to seasonal (S2S) program initialized in 2013 by WCRP and WWRP. Recent studies have shown that this forecast system is among the best at predicting sudden stratospheric warming (SSW) events in two hemispheres (Domeisen et al., 2020a, 2020b; Rao et al., 2019, 2020a, 2020b). A full ozone photochemistry scheme is not used in many S2S or seasonal forecast models due to its computational expense, but CFSv2 includes a prognostic ozone parameterization scheme (Compo et al., 2016). Specifically, the time tendency of ozone is specified using the partial CHEM2D Ozone Photochemistry Parameterization (CHEM2D-OPP) method (McCormack et al., 2006).

Considering that Arctic ozone hole events in March are persistent with little sub-monthly variability, we focus on the seasonal forecast of the three ozone hole events, rather than the day-by-day forecasts in details. The CFSv2 initializations at the very beginning of each winter month are downloaded and assessed in this study (Table S1). Similar to the winds, height, and air temperature, the total column ozone is also a standard

output from the forecast system.

2.2 Reanalysis and observations

The ERA5 reanalysis (Hersbach et al., 2020) is used as the baseline for assessment of the CFSv2 forecasts. The daily and monthly data at a 1.5°×1.5° horizontal resolution is downloaded from the Copernicus Climate Change Service Climate Data Store after registration (https://cds.climate.copernicus.eu). Variables used in this study include the zonal and meridional winds, air temperature, geopotential (divided by the gravitational acceleration to extract the height), and Ertel potential vorticity at 37 pressure levels (1000–1hPa). The total column ozone (TCO3) is not provided by ERA5, but it can be computed by vertically integrating the ozone mixing ratio (RO3) divided by the gravitational acceleration: $\mathrm{TCO3} = \frac{1}{g}\iint_{Ps}^{0} \mathrm{RO3}\, dp$, where Ps is the surface pressure, and g is the gravitational acceleration constant (g = 9.8 m/s^2) The units of the TCO3 is converted from kg/m^2 to Dobson Unit (DU) with a rough estimate of 1 DU = 2.1415 × 10^{-5} kg/m^2 (http://www.temis.nl/general/dobsonunit.html; Zhang et al., 2019). ERA5 assimilates 19 different ozone observation sources during different periods since 1979 (Fig. 7 in Hersbach et al., 2020), so it is reasonable to use TCO3 from this modern reanalysis as a reference state.

The monthly Niño3.4 index is used to identify the phase of the El Niño-Southern Oscillation (ENSO). The sea surface temperature (SST) data are collected by the Japanese Meteorological Agency (COBE SST) and sourced from PSL, NOAA (https://psl.noaa.gov/data/gridded/data.cobe.html). In addition, the quasi biennial oscillation (QBO) time series shared by Berlin Free University (https://www.geo.fu-berlin.de/en/met/ag/strat/produkte/qbo/index.html) is also used to test the potential predictability source.

2.3 Methods

To assess the predictability of ozone and circulation anomaly distributions, the pattern correlation coefficient (PCC) between forecasts and the reanalysis for a variable V is utilized, $\mathrm{PCC} = \frac{\sum_{i=1}^{n} w(i)[V_{\mathrm{FC}}(i)-\overline{V_{\mathrm{FC}}}][V_{\mathrm{RE}}(i)-\overline{V_{\mathrm{RE}}}]}{\sqrt{\sum_{i=1}^{n} w(i)[V_{\mathrm{FC}}(i)-\overline{V_{\mathrm{FC}}}]^2}\sqrt{\sum_{i=1}^{n} w(i)[V_{\mathrm{RE}}(i)-\overline{V_{\mathrm{RE}}}]^2}}$. In the PCC formula, i is the spatial grid index, n is the total number of spatial grid points in the extratropics (30–90°N). The subscript "FC" denotes the model forecast, and "RE" denotes the ERA5 reanalysis. The overbars in the PCC formula denote spatial averages.

The following metrics are used to track the relationship between the stratospheric polar vortex and the Arctic total ozone: (1) the polar cap height area-weighted over 60–90°N at 50hPa; (2) polar total ozone area-weighted over 60–90°N [Strahan et al. (2013) used the 63–90°N means]; (3) days of strong polar vortex during December–February (DJF) with the zonal-mean zonal winds at 60°N and 10hPa greater than 35 or 40 m/s; (4) another metric for the polar vortex strength, zonal-mean zonal winds at 60°N and 10hPa in DJF; (5) the volume of the polar stratospheric clouds (V_{PSC}) in late winter (February–March, FM), estimated as

$V_{PSC} = (0.8 \times A_{PSC}@50\text{hPa} + 0.2 \times A_{PSC}@30\text{hPa}) \times 5.06\text{km}$, where A_{PSC}@50hPa is the area at 50 hPa colder than 195.59 K and A_{PSC}@30hPa is the area at 30hPa colder than 193.61 K (Rex et al., 2004; Rieder & Polvani, 2013; Garfinkel et al., 2015). The third and fifth indices are calculated using the ERA5 daily means, and the others are based on the monthly means.

3. Backgrounds for the three historical Artic ozone holes

Figure 1 shows the time series of several metrics, including the Arctic total column ozone versus polar cap height at 50 hPa in March (Figure 1a), days of strong polar vortex in DJF (Figure 1b), the winter-mean polar jet intensity versus late winter V_{PSC} (Figure 1c), and two dominant tropical forcings (ENSO and QBO). It is evident that polar cap height and ozone in March 1997, 2011, and 2020 rank as the top three low values from 1979–2020 (Figure 1a). The high correlation (i.e., 0.80) between polar cap height and the Arctic total ozone might indicate that they are strongly coupled with each other. Based on this, Seviour et al. (2014) designed a statistical plus dynamical forecast procedure but for seasonal prediction of the Antarctic ozone, although the GloSea5 forecast system does not include a diagnostic chemical module. The formation of low Arctic ozone concentrations is also preceded by a quiescent winter with a strong stratospheric polar vortex (Figures 1b, 1c), indicating a weak residual circulation (not shown). A strong and cold polar vortex allows for the formation of more polar stratospheric clouds (Figure 1c) and chlorine activation (Manney et al., 2011; Arnone et al., 2012), whereby the depletion of ozone is larger than normal. In addition, no midwinter SSW appeared before the three ozone hole events, and the final warming did not happen until April (e.g., 30 April 1997, 5 April 2011, 29 April 2020). Our results do not suggest any directly significant relationship between ENSO and the Arctic total ozone, but the QBO indeed contributes marginally to interannual variability of March ozone (Figure 1d). Hurwitz et al. (2011) also emphasize the possible impact of warm SST anomalies in North Pacific on the strong polar vortex in March 2011, which were not observed in the 1996/97 and 2019/20 winters (not shown).

Figure 2 compares the meteorological conditions for the three Arctic ozone hole events. The climatological ozone is around 420 DU in March (Figure 2a), but the lowest column-ozone is below 280 DU for the three holes (Figures 2b–2d). The minimum ozone value over the Arctic in March 2020 is even lower than in 2011 and 1997, and the position of the low center is also different among the events: towards North America in March 2020, symmetric about the pole in March 2011, but towards Eurasia in March 1997. Such a displacement of the low-ozone center is consistent with the shape of the stratospheric polar vortex at 10hPa (similar at 50hPa) denoted by the high PV value (Figures 2e–2h) and low height anomalies at 50 hPa (Figure S1). On average, the polar vortex begins to weaken or collapse in March (Figures 2e, S1). However, in March 1997, 2011, and 2020, the polar vortex was still strong, manifested by the large PV values in the Arctic at 10 hPa (>600 PVU). The PV maximum was located in Arctic Canada in March 2020, near the North Pole in March 2011, and shifted towards Arctic Russia in March 1997 (Figures 2f–2h). Therefore, the Arctic ozone hole is coupled with an extremely strong stratospheric polar vortex.

Climatologically, temperatures over the Arctic at 50hPa in March are 210–215K, well above the threshold for polar stratospheric cloud formation (Figure 2i). In March 2020, 2011, and 1997, the coldest temperature anomalies in the Arctic stratosphere reached ~-18K, cold enough to allow for heterogeneous ozone depletion (Figures 2j–2l) that occurs more often in the Antarctic and initializes radiative-dynamic feedbacks that allow the cold temperatures and strong vortex to persist (Randel & Wu, 1999).

The residual (or Brewer-Dobson) circulation dynamically transports mass from the ozone-rich tropics to the ozone-poor extratropics (Figure 2m). The strong polar vortex with strong westerly jet (Figures 2i–2l) suppresses the upward propagation of waves and therefore the wave-forced residual mass circulation and mixing, as is evident by the positive ozone mixing ratio anomalies in tropics and negative anomalies in extratropics (Figure 2n–2p). To summarize, both chemical and dynamical processes associated with a strong polar vortex contributed to the formation of the Arctic ozone holes in 1997, 2011, and 2020.

4. Prediction of the Arctic ozone holes in CFSv2

The predictions of the March total ozone and the geopotential height (PV at pressure levels is unavailable for CFSv2) anomalies from initializations at the beginning of February and March are shown in Figure 3. While the early forecasts correctly forecast the sign of the ozone anomalies, the anomaly amplitudes are largely underestimated (Figures 3a, 3c, 3e). The early initializations better capture the 2011 ozone hole (central low: ~-80 DU) than the 1997 and 2020 ozone holes (central low: ~-40 DU), indicating a different predictability of ozone loss for the three events. The late initializations have a similar predictive skill for the three ozone holes, with a pattern correlation around 0.9 (Figures 3b, 3d, 3f). The distribution of the column-ozone is largely controlled by the polar vortex both in the reanalysis (shadings) and in forecasts (contours; Figures 3g–3l). The low centers of the column-ozone and height anomalies are closely situated. The predictability of the column-ozone is highly consistent with that of stratospheric height: the strong polar vortex in March 2011 is well forecasted in the early-February initializations (Figure 3i), which exceeds the average predictive limit (~ two weeks) of stratospheric strong polar vortex (Domeisen et al., 2020a).

Rao et al. (2019, 2020b) reported that favorable external forcings such as ENSO and QBO can increase the predictive limit for some SSWs. It is noticeable that the mild cold ENSO state and the QBO westerly winds (Figure 1d) in the 2010/11 winter together increase the possibility of a strong polar vortex in forecasts. The ENSO and QBO were nearly neutral in the 1996/97 and 2019/20 winters, and the polar vortex anomalies are accurately forecasted only for March initializations (Figures 3h, 3j, 3l).

For a forecast system without a chemical module and ozone output, the prediction of ozone can be derived from a variable coupled with the ozone, e.g., the polar vortex strength. An empirical prediction of the Arctic total ozone using the forecasted polar cap height (see Figure S2) is shown in Figure 4. Based on the ERA5 reanalysis, the simultaneous linear relationship between height and ozone is established (Figure 4a), which can then be used to predict (in an empirical manner) Arctic total ozone. Figures 4c–4e assess the skill of such an

empirical ozone predictive model. The empirical prediction model underestimates the extremity of the low-ozone in initializations earlier than March, but the empirical model can well reproduce the observed anomalies in the latest initializations (March). The earlier initializations (November–January) contain little skill at forecasting the ozone hole in March, except that the initializations in February 2011 still have high skill possibly due to the cold ENSO and westerly QBO conditions. We also assess sensitivity to basing the empirical model on the regression between V_{PSC} in late winter (February–March) and the Arctic total ozone (Figure 4b), and no improvement is found (not shown). Overall, the statistical model might have some skill in forecasting seasonal mean polar ozone (e.g., Seviour et al., 2014), but its predictive skill is too low for the March ozone hole event to reach the "hole" criterion for earlier initializations.

The direct prediction of ozone from the chemical module in CFSv2 is similar to the empirical prediction (Figure 5). For initializations at the beginning of March, nearly all of the Arctic ozone anomalies can be reproduced by CFSv2 (Figures 5a–5c). For initializations in early February 2011, most of the negative Arctic ozone anomalies in March 2011 are forecasted (Figure 5b). The pattern correlation of the extratropical total ozone is also much larger for initializations in March than other winter months (Figures 5d–5f). These results suggest that March Arctic ozone hole events can be accurately predicted on March 1 or earlier.

5. Conclusions

Since 1979, three March ozone holes have been observed with a monthly minimum of Arctic total ozone lower than 280 DU: 1997, 2011, and 2020. Unlike the Antarctic ozone hole that has formed every spring since the 1980s, an Arctic ozone hole has happened only every one or two decades. A timely and accurate warning of the formation of ozone hole is of vital importance for ecosystems in subpolar regions. Namely, reduced ozone in the stratosphere lets more ultraviolet radiation reach the near surface and harm life in high latitudes after the spring equinox. Based on the ERA5 reanalysis, observations, and seasonal forecasts by CFSv2, the meteorological backgrounds of the historical Arctic ozone holes and their predictability using an empirical model and a dynamical model are assessed.

Some similarities are found for the three ozone hole events: 1) No midwinter SSWs happened before the March ozone hole events, which is consistent with the extremely strong polar vortex throughout the winter, as well as more days in DJF with a strong westerly jet and with extremely cold temperatures that allow for polar stratospheric clouds to form (denoted by large V_{PSC}). 2) The final warming occurred in April for the three ozone hole events, after the ozone hole already had time to develop. 3) The ozone low center is mainly controlled by the simultaneous polar vortex shape: displaced towards Canada and Greenland during March 2020, symmetrically distributed about the North Pole during March 2011, and displaced towards Arctic Russia during March 1997. 4) A dipole stratospheric ozone mixing ratio anomaly pattern was found for ozone hole events, that is, the positive ozone anomaly in the tropical stratosphere is contrasted with the negative ozone anomaly in the extratropical

stratosphere.

Differences are also evident: 1) The backgrounds are different for the three ozone holes, with the March 2011 ozone hole happening following a moderate cold ENSO state and a weak QBO westerly in winter. However, the ENSO and QBO were nearly neutral in the 1996/97 and 2019/20 winters. 2) The 2011 ozone hole event may have been more predictable than the other two due to favorable conditions for a strong stratospheric polar vortex.The CFSv2 is among the best models at predicting the stratospheric evolution (Domeisen et al., 2020a, 2020b; Garfinkel et al., 2020; Rao et al., 2019, 2020a, 2020b), and hence we expect that our conclusions will be representative of other state-of-the-art models with a chemistry module.

We also find that the ozone predicted from an empirical model using model output is nearly as skillful as ozone actually predicted by the model itself. This similarity implies that one can use models in the S2S archive (which do not archive ozone) to study predictability of ozone hole events. Namely, the intensity of the stratospheric polar vortex in March and V_{PSC} calculated based on temperatures, are a good substitute index for Arctic ozone prediction. We leave for future work a more detailed study of empirical prediction of ozone based on forecasted polar vortex metrics in other S2S models.

Acknowledgements

The authors acknowledge the National Key R&D Program of China (2016YFA0602104) and the National Natural Science Foundation of China (41705024). This research was also supported by the ISF-NSFC joint research program (3259/19), and the European Research Council starting grant under the European Unions Horizon 2020 research and innovation programme (677756). The authors thank the ECMWF and CPC for providing the ERA5 reanalysis (https://cds.climate.copernicus.eu) and CFSRv2 forecasts (https://www.ncdc.noaa.gov/data-access/model-data/model-datasets/climate-forecast-system-version2-cfsv2) data, respectively. The SST data are compiled by the JMA and redistributed by PSL, NOAA (https://psl.noaa.gov/data/gridded/data.cobe.html). The QBO observations are collected and updated by Berlin Free University (https://www.geo.fu-berlin.de/en/met/ag/strat/produkte/qbo/index.html).

References

Arnone, E., Castelli, E., Papandrea, E., Carlotti, M., & Dinelli, B. M. (2012). Extreme ozone depletion in the 2010-2011 Arctic winter stratosphere as observed by MIPAS/ENVISAT using a 2-D tomographic approach. *Atmospheric Chemistry and Physics, 12*(19), 9149–9165. https://doi.org/10.5194/acp-12-9149-2012

Calvo, N., Polvani, L. M., & Solomon, S. (2015). On the surface impact of Arctic stratospheric ozone extremes. *Environmental Research Letters, 10*(9), 094003. https://doi.org/10.1088/1748-9326/10/9/094003

Chipperfield, M. P., Dhomse, S. S., Feng, W., McKenzie, R. L., Velders, G. J. M., & Pyle, J. A. (2015). Quantifying the ozone and ultraviolet benefits already achieved by the

Montreal Protocol. *Nature Communications, 6*, 7233. https://doi.org/10.1038/ncomms8233

Compo, G. P, Moorthi, S. Lu, S., Long, C. S., Lee, H. T., McCormack, J. P., Sardeshmukh, P. D., & Whitaker, J. S. (2016). Improving the prognostic ozone parameterization in the NCEP GFS and CFS for climate reanalysis and operational forecasts. Paper presented at *28th Conference on Climate Variability and Change* (a session of *96th American Meteorological Society Annual Meeting*), American Meteorological Society, New Orleans, Louisiana.

Domeisen, D. I. V., Butler, A. H., Charlton-Perez, A. J., Ayarzagüena, B., Baldwin, M. P., Dunn-Sigouin, E., . . . Taguchi, M. (2020a). The Role of the stratosphere in subseasonal to seasonal prediction: 1. Predictability of the stratosphere. *Journal of Geophysical Research: Atmospheres, 125*(2), e2019jd030920. https://doi.org/10.1029/2019jd030920

Domeisen, D. I. V., Butler, A. H., Charlton-Perez, A. J., Ayarzagüena, B., Baldwin, M. P., Dunn-Sigouin, E., . . . Taguchi, M. (2020b). The role of the stratosphere in subseasonal to seasonal Prediction: 2. Predictability arising from stratosphere-troposphere coupling. *Journal of Geophysical Research: Atmospheres, 125*(2), e2019jd030923. https://doi.org/10.1029/2019jd030923

Garfinkel, C. I., Hurwitz, M. M., & Oman, L. D. (2015). Effect of recent sea surface temperature trends on the Arctic stratospheric vortex. *Journal of Geophysical Research: Atmospheres, 120*(11), 5404–5416. https://doi.org/10.1002/2015jd023284

Garfinkel, C. I., Schwartz, C., White, I. P., & Rao, J. (2020). Predictability of the early winter Arctic Oscillation from Autumn Eurasian snowcover in subseasonal forecast models. *Climate Dynamics*, in press.

Harari, O., Garfinkel, C. I., Ziskin Ziv, S., Morgenstern, O., Zeng, G., Tilmes, S., . . . Davis, S. (2019). Influence of Arctic stratospheric ozone on surface climate in CCMI models. *Atmospheric Chemistry and Physics*, *19*(14), 9253–9268. https://doi.org/10.5194/acp-19-9253-2019

Harris, N. R. P., Lehmann, R., Rex, M., & von der Gathen, P. (2010). A closer look at Arctic ozone loss and polar stratospheric clouds. *Atmospheric Chemistry and Physics, 10*(17), 8499–8510. https://doi.org/10.5194/acp-10-8499-2010

Hersbach, H., Bell, B., Berrisford, P., Hirahara, S., Horányi, A., Muñoz-Sabater, J., . . . Thépaut, J. N. (2020). The ERA5 Global Reanalysis. *Quarterly Journal of the Royal Meteorological Society*. https://doi.org/10.1002/qj.3803

Hommel, R., Eichmann, K. U., Aschmann, J., Bramstedt, K., Weber, M., von Savigny, C., . . . Burrows, J. P. (2014). Chemical ozone loss and ozone mini-hole event during the Arctic winter 2010/2011 as observed by SCIAMACHY and GOME-2. *Atmospheric Chemistry and Physics, 14*(7), 3247–3276. https://doi.org/10.5194/acp-14-3247-2014

Hurwitz, M. M., Newman, P. A., & Garfinkel, C. I. (2011). The Arctic vortex in March 2011: a dynamical perspective. *Atmospheric Chemistry and Physics, 11*(22), 11447–11453. https://doi.org/10.5194/acp-11-11447-2011

Ivy, D. J., Solomon, S., Calvo, N., & Thompson, D. W. J. (2017). Observed connections of Arctic stratospheric ozone extremes to Northern Hemisphere surface climate.

Environmental Research Letters, *12*(2), 024004. https://doi.org/10.1088/1748-9326/aa57a4

Liu, N. Q., Huang, F. X., & Wang, W. H. (2011). Monitoring of the 2011 spring low ozone events in the Arctic region. *Chinese Science Bulletin*, *56*(27), 2893–2896. https://doi.org/10.1007/s11434-011-4636-3

Manney, G. L., Santee, M. L., Rex, M., Livesey, N. J., Pitts, M. C., Veefkind, P., . . . Zinoviev, N. S. (2011). Unprecedented Arctic ozone loss in 2011. *Nature*, *478*(7370), 469–475. https://doi.org/10.1038/nature10556

McCormack, J. P., Eckermann, S. D., Siskind, D. E., & McGee, T. J. (2006). CHEM2D-OPP: A new linearized gas-phase ozone photochemistry parameterization for high-altitude NWP and climate models. *Atmospheric Chemistry and Physics*, *6*(12), 4943–4972. https://doi.org/10.5194/acp-6-4943-2006

Neely, R. R., Marsh, D. R., Smith, K. L., Davis, S. M., & Polvani, L. M. (2014). Biases in southern hemisphere climate trends induced by coarsely specifying the temporal resolution of stratospheric ozone. *Geophysical Research Letters*, *41*(23), 8602–8610. https://doi.org/10.1002/2014gl061627

Newman, P. A., Gleason, J. F., McPeters, R. D., & Stolarski, R. S. (1997). Anomalously low ozone over the Arctic. *Geophysical Research Letters*, *24*(22), 2689–2692. https://doi.org/10.1029/97gl52831

Olascoaga, M. J., Brown, M. G., Beron-Vera, F. J., & Koçak, H. (2012). Brief communication "Stratospheric winds, transport barriers and the 2011 Arctic ozone hole&quot. *Nonlinear Processes in Geophysics*, *19*(6), 687–692. https://doi.org/10.5194/npg-19-687-2012

Previdi, M., & Polvani, L. M. (2014). Climate system response to stratospheric ozone depletion and recovery. *Quarterly Journal of the Royal Meteorological Society*, *140*(685), 2401–2419. https://doi.org/10.1002/qj.2330

Randel, W. J., & Wu, F. (1999). A stratospheric ozone trends data set for global modeling studies. *Geophys. Res. Lett.*, *26*(20), 3089–3092. https://doi/org/10.1029/1999gl900615

Rao, J., Garfinkel, C. I., Chen, H., & White, I. P. (2019). The 2019 New Year stratospheric sudden warming and its real-time predictions in multiple S2S models. *Journal of Geophysical Research: Atmospheres*, 124(21), 11155–11174. https://doi/org/10.1029/2019JD030826

Rao, J., Garfinkel, C. I., & White, I. P. (2020). Predicting the downward and surface influence of the February 2018 and January 2019 sudden stratospheric warming events in Subseasonal to Seasonal (S2S) models. *Journal of Geophysical Research: Atmospheres*, 125(2), e2019JD031919. https://doi/org/10.1029/2019JD031919

Rao, J., Garfinkel, C. I., White, I. P., & Schwartz, C. (2020b). The Southern Hemisphere sudden stratospheric warming in September 2019 and its predictions in S2S models. *Journal of Geophysical Research: Atmospheres*.

Rex, M., Salawitch, R. J., von der Gathen, P., Harris, N. R. P., Chipperfield, M. P., & Naujokat, B. (2004). Arctic ozone loss and climate change. *Geophysical Research Letters*, *31*(4), L04116. https://doi.org/10.1029/2003gl018844

Rex, M., Salawitch, R. J., Deckelmann, H., von der Gathen, P., Harris, N. R. P., Chipperfield, M. P., . . . Zerefos, C. (2006). Arctic winter 2005: Implications for stratospheric ozone loss and climate change. *Geophysical Research Letters, 33*(23), L23808. https://doi.org/10.1029/2006gl026731

Rieder, H. E., & Polvani, L. M. (2013). Are recent Arctic ozone losses caused by increasing greenhouse gases? *Geophysical Research Letters, 40*(16), 4437–4441. https://doi.org/10.1002/grl.50835

Rieder, H. E., Polvani, L. M., & Solomon, S. (2014). Distinguishing the impacts of ozone-depleting substances and well-mixed greenhouse gases on Arctic stratospheric ozone and temperature trends. *Geophysical Research Letters, 41*(7), 2652–2660. https://doi.org/10.1002/2014gl059367

Saha, S., Moorthi, S., Wu, X., Wang, J., Nadiga, S., Tripp, P., . . . Becker, E. (2014). The NCEP climate forecast system version 2. *Journal of Climate, 27*(6), 2185–2208. https://doi.org/10.1175/jcli-d-12-00823.1

Seviour, W. J. M., Hardiman, S. C., Gray, L. J., Butchart, N., MacLachlan, C., & Scaife, A. A. (2014). Skillful seasonal prediction of the Southern Annular mode and Antarctic ozone. *Journal of Climate, 27*(19), 7462–7474. https://doi.org/10.1175/jcli-d-14-00264.1

Shaw, T. A., & Perlwitz, J. (2014). On the control of the residual circulation and stratospheric temperatures in the Arctic by planetary wave coupling. *Journal of the Atmospheric Sciences, 71*(1), 195–206. https://doi.org/10.1175/jas-d-13-0138.1

Sinnhuber, B. M., Stiller, G., Ruhnke, R., von Clarmann, T., Kellmann, S., & Aschmann, J. (2011). Arctic winter 2010/2011 at the brink of an ozone hole. *Geophysical Research Letters, 38*(24), L24814. https://doi.org/10.1029/2011gl049784

Solomon, S., Haskins, J., Ivy, D. J., & Min, F. (2014). Fundamental differences between Arctic and Antarctic ozone depletion. *Proceedings of the National Academy of Sciences of the United States of America, 111*(17), 6220–6225. https://doi.org/10.1073/pnas.1319307111

Solomon, S. (1999). Stratospheric ozone depletion: A review of concepts and history. *Reviews of Geophysics, 37*(3), 275–316. https://doi.org/10.1029/1999rg900008

Strahan, S. E., Douglass, A. R., & Newman, P. A. (2013). The contributions of chemistry and transport to low arctic ozone in March 2011 derived from Aura MLS observations. *Journal of Geophysical Research: Atmospheres, 118*(3), 1563–1576. https://doi.org/10.1002/jgrd.50181

Thompson, D. W., & Solomon, S. (2002). Interpretation of recent Southern Hemisphere climate change. *Science, 296*(5569), 895–899. https://doi.org/10.1126/science.1069270

Varotsos, C. A., Cracknell, A. P., & Tzanis, C. (2012). The exceptional ozone depletion over the Arctic in January-March 2011. *Remote Sensing Letters, 3*(4), 343–352. https://doi.org/10.1080/01431161.2011.597792

Waugh, D. W., Oman, L., Newman, P. A., Stolarski, R. S., Pawson, S., Nielsen, J. E., & Perlwitz, J. (2009). Effect of zonal asymmetries in stratospheric ozone on simulated Southern Hemisphere climate trends. *Geophysical Research Letters, 36*(18), L18701. https://doi.org/10.1029/2009gl040419

456 Zhang, Y., Wang, W., Li, X., Zhang, X., Zheng, Z., & Liu, R. (2013). Anomalously low
457 ozone of 1997 and 2011 Arctic spring: Monitoring results and analysis. *Advances in*
458 *Polar Science*, *23*(2), 82–86. https://doi.org/10.3724/sp.J.1085.2012.00082
459 Zhang, Z. Rao, J., Guo, D., Zhang, W., Li, L., Tang, Z., Shi, C., Su, Y., & Zhang, F. (2019).
460 Interdecadal variations of the midlatitude ozone valleys in summer. *Atmosphere*, 10(11),
461 677. https://doi/org/10.3390/atmos10110677
462

Figures and captions

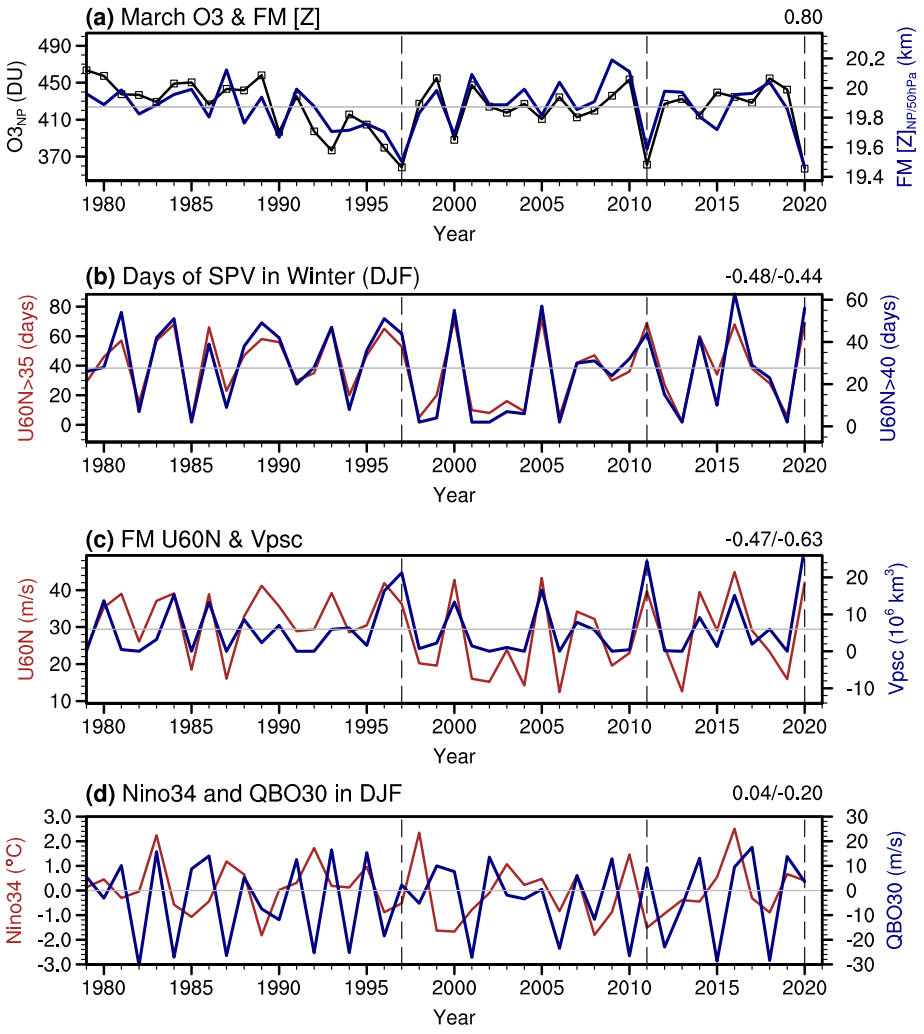

Figure 1. (a) Time series of the polar (60–90°N) ozone (units: DU, left ordinate) in March and 50-hPa height (units: km, right column) in late winter (February–March, FM hereafter) from 1979–2020 in the ERA5 reanalysis. (b) Days of strong polar vortex in December–February (DJF) with the zonal mean zonal wind at 10hPa and 60°N greater than 35 m/s (left ordinate) and 40 m/s (right ordinate), respectively. (c) Time series of the zonal mean zonal wind in FM at 10hPa and 60°N and the volume of polar stratospheric clouds (V_{PSC}) in FM. (d) The time series of the winter-mean Niño3.4 index (units: °C, left ordinate) and the QBO index (units: m/s, right ordinate) at 30 hPa (QBO30). The correlation between each index and the March ozone is also printed on the top right in each plot.

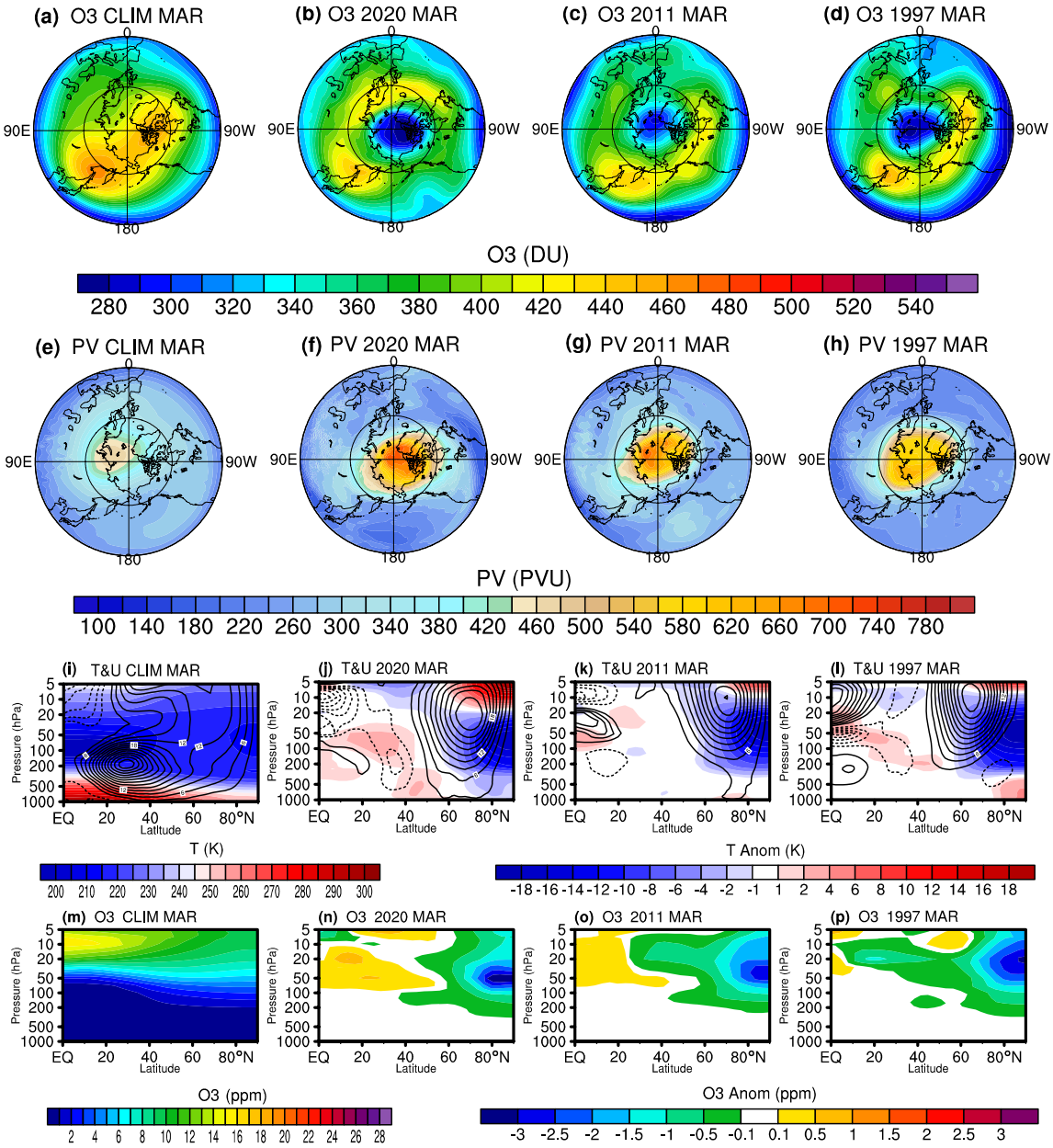

Figure 2. (a–d) The climatological distribution of March ozone (units: DU) in the extratropics and three historical March ozone hole events in 1997, 2011, and 2020, respectively. (e–f) As in (a–d) but for the distribution of the March potential vorticity (PV). (i) Latitude-pressure cross section of the climatological zonal-mean temperature (shadings, units: K) and zonal-mean zonal wind (contours, units: m/s) in March. (j–l) As in (i) but for the temperature and zonal wind anomalies in March 1997, 2011, and 2020, respectively. (m–p) As in (i–l) but for the latitude-pressure cross section of the ozone concentration (units: ppm). Note that the climatology (i, m) and anomalies (j–l, n–p) in the last two rows use different color scales.

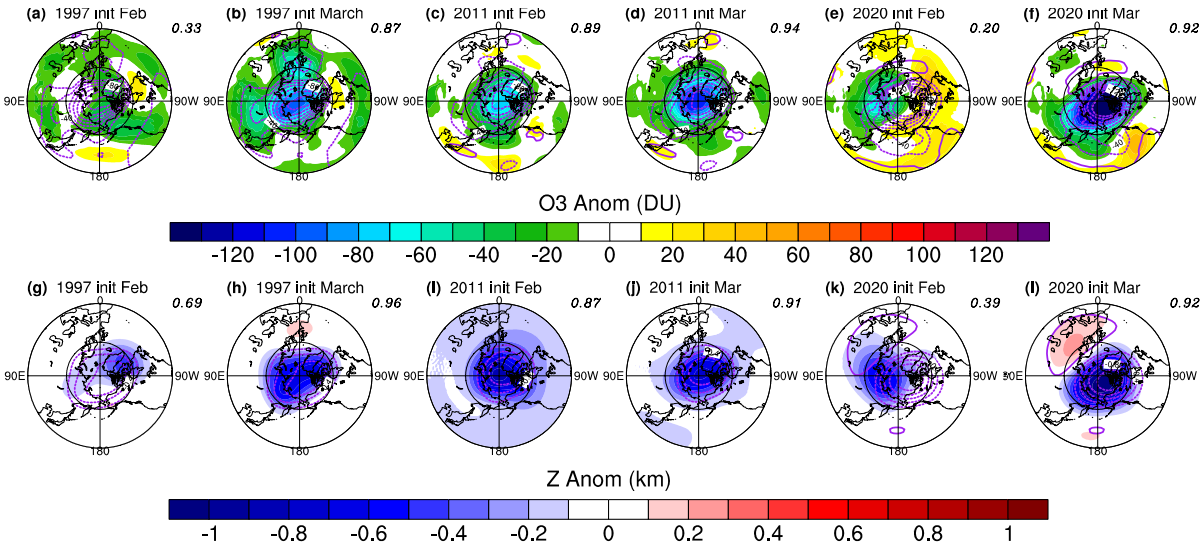

Figure 3. (a). CFSv2 predictions of the total ozone anomalies (first row, units: DU) and height anomalies at 50 hPa (second row, units: km) in shadings. The contours show the observed anomalies from the ERA5 reanalysis, with an ozone interval of 20 DU and height interval of 0.2 km (zero skipped). The first two columns (a, b, g, h) show predictions for the 1997 March ozone hole, the middle two columns (c, d, i, j) show predictions for the 2011 March ozone hole, and the last two columns (e, f, k, l) show prediction for the 2020 March ozone hole. Only predictions initialized at the beginning of February (a, c, e, g, i, k) and March (b, d, f, h, j, l) are shown.

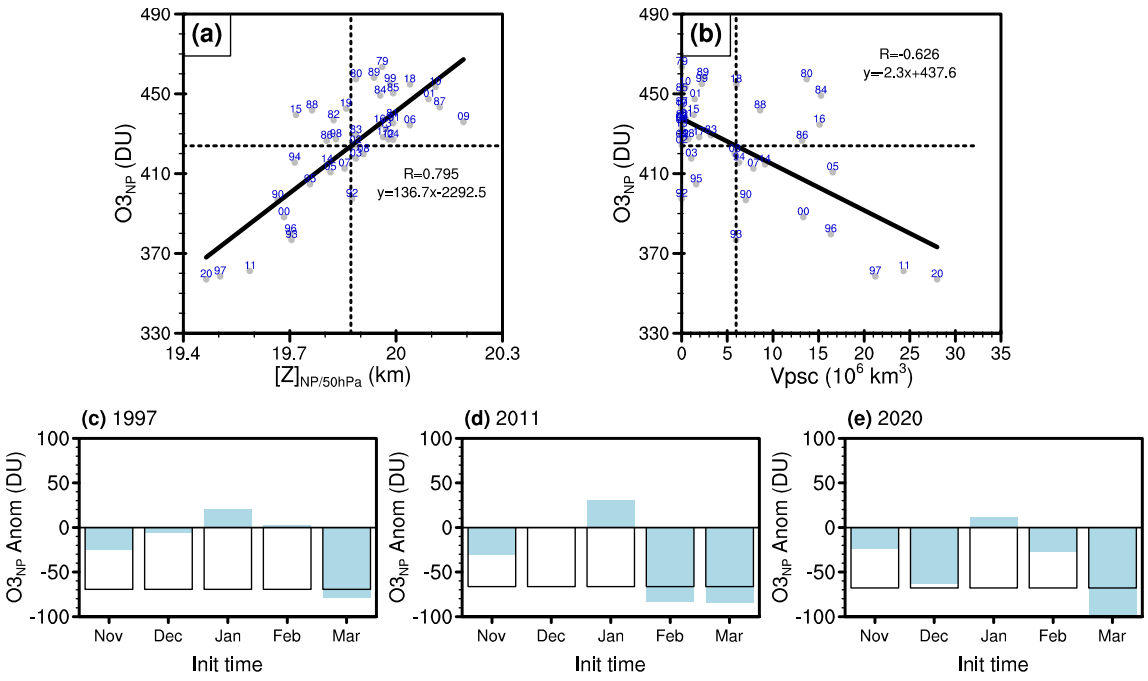

Figure 4. (a) Scatterplot of the polar cap height at 50hPa in FM (units: km) versus the polar cap total ozone in March (units: DU). The year is marked with a two-digital integer. The horizontal and vertical dashed lines are the mean of the March polar cap height at 10 hPa and total ozone, respectively. The thick line is the linear regression between the height and total ozone. (b) As in (a) but for scatterplot of the volume of polar stratospheric clouds in FM (V_{PSC}; units: $10^6 km^3$) versus the total ozone area-averaged over the polar cap region in March. (c–e) Empirical predictions of the polar cap total ozone in March (units: DU) using the forecasted polar cap height anomalies (i.e., 137.6 × height anomalies). The empirical predictions of the polar cap total ozone in March using the forecasted V_{PSC} anomalies are similar (not shown).

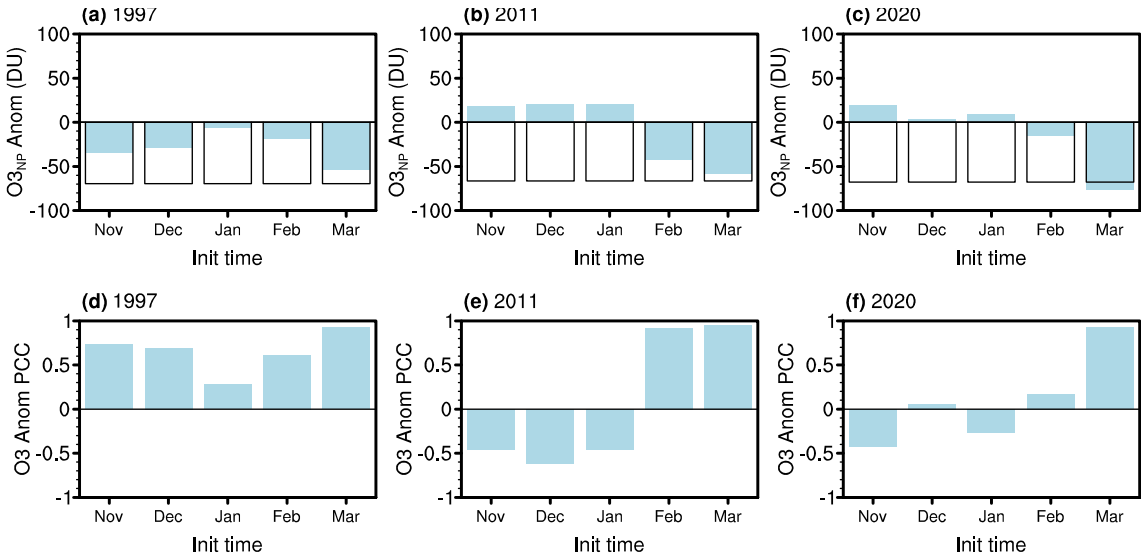

508

509 **Figure 5.** (a–c) CFSv2 predictions of the total ozone anomalies (units: DU) in March over the
510 polar cap (60–90°N) for the three historical ozone hole events in 1997, 2011, and 2020. The
511 abscissa shows the initialization time at the beginning of each month, and four members are
512 available. The filled histogram shows the forecast, and the unfilled histogram shows the
513 ERA5 reanalysis. (d–f) As in (a–c) but for pattern correlations between the forecasts and the
514 reanalysis.